optica

Architecture for the photonic integration of an optical atomic clock: supplementary material

Zachary L. Newman,[1,*] Vincent Maurice,[1] Tara Drake,[1] Jordan R. Stone,[1,2] Travis C. Briles,[1] Daryl T. Spencer,[1] Connor Fredrick,[1,2] Qing Li,[3] Daron Westly,[3] B. R. Ilic,[3] Boqiang Shen,[4] Myoung-Gyun Suh,[4] Ki Youl Yang,[4] Cort Johnson,[5] David M. S. Johnson,[5] Leo Hollberg,[6] Kerry J. Vahala,[4] Kartik Srinivasan,[3] Scott A. Diddams,[1,2] John Kitching,[1] Scott B. Papp,[1,2] Matthew T. Hummon[1]

[1]*National Institute of Standards and Technology, Boulder, CO, 80305 USA*
[2]*Department of Physics, University of Colorado Boulder, Boulder, CO 80309, USA*
[3]*Center for Nanoscale Science and Technology, National Institute of Standards and Technology, Gaithersburg, MD, 20899 USA*
[4]*California Institute of Technology, Pasadena, CA, 91125 USA*
[5]*Charles Stark Draper Laboratories, Cambridge, MA, 02139*
[6]*Stanford University, Stanford, CA 94305*
**Corresponding author: zachary.newman@nist.gov*

Published 20 May 2019

This document provides supplementary information to "Architecture for the photonic integration of an optical atomic clock," https://doi.org/10.1364/OPTICA.6.000680.

1. Microfabricated clock components

1.1 Microfabricated vapor cell

The rubidium vapor cell is composed of a 10×10×3 mm silicon frame sandwiched between two 700 μm-thick aluminosilicate glass pieces. The silicon frame is fabricated by deep reactive ion etching of a blank silicon wafer and features a main chamber 3×3 mm and an ancillary chamber 1.5×1.5 mm that are connected through 125 μm-wide baffles. The glass windows are anodically bonded to the silicon frame. Before bonding the second window under vacuum, a rubidium dispensing pill (natural abundance) is introduced in the ancillary chamber along with a piece of non-evaporable getter. Rubidium is then released into the cell by heating the dispensing pill with a focused laser beam [1]. Helium diffusion through the glass windows (up to atmospheric concentration) as the cell ages accounts for ≈100 kHz of broadening and <10 kHz of broadening is due to unwanted gases that arise during the cell bonding and filling process not pumped by the getter [2].

We have measured the absolute frequency of our clock to be $\nu \approx 385\,284\,566\,347\,789 \pm 30$ Hz, which corresponds to a frequency shift from the accepted value of the two-photon transition frequency of $\Delta\nu \approx -22.7$ kHz [3] and is primarily due to the light shift and the collision shift. Table (S1) gives a conservative estimate of the uncertainty budget for our clock. We have measured the light shift to be ≈-1.5 kHz/mW, resulting in a ≈-23.4 kHz shift for the 15.6 mW of clock laser power. We have also measured the Rb-Rb self-collision shift to be ≈-192.6 Hz/K near the cell temperature (100°C) which is consistent with Ref. [2]. Accounting for these shifts, we measure an absolute frequency shift of $\Delta\nu \approx 2.9 \pm 7.9$ kHz relative to Ref. [3], or a fractional frequency shift of $\Delta\nu/\nu \approx 8\times10^{-12}$. We expect a ≈4 kHz collision shift from helium diffusion and we determine the maximum background gas pressure shift by applying the shift/broadening rates measured in Ref. [2] to our estimate of background gas pressure. Both the helium collision shift and the background gas collision shift are consistent with our ≈100 kHz collision broadening measurement.

Based on our linewidth measurements we estimate that the background gas pressure in a given cell could vary up to ~1 mTorr and is the main contribution to the uncertainty budget for our clock. With improvements in cell fabrication techniques, both the helium and background gas shifts could, in principle, be reduced significantly. We expect electronic shifts due to residual amplitude modulation of the clock laser and offsets at the output of the lock-in detector used in the atomic lock to influence the clock frequency. Although these were not measured, we estimate the uncertainty in the clock frequency due to electronic shifts by measuring the slope of the error signal used to lock the clock laser to the atoms and multiplying by the output offset of the lock-in detector.

Fig. S1 summarizes the record of absolute frequency measurements of the ^{87}Rb, 5S→5D, F=2→ F'=4 worldwide.

Frequency measurements prior to 2005 were made using a frequency chain while measurements made thereafter were made with an optical frequency comb.

1.2 Silica microresonator

Fig. 1c shows an image of the wedged, 21.97 GHz free-spectral range silica (SiO_2) microresonator used to measure the repetition rate of our self-referenced Si_3N_4 microcomb. The design, fabrication and implementation of the silica comb has been described in detail elsewhere [4]. Briefly, the microresonator is fabricated by thermally growing a layer of SiO_2 on a silicon substrate. The silica layer is then shaped into a wedge-resonator by lithographically patterning a photoresist material and etching the silica with a hydrofluoric acid solution. As a final step, the pedestal is formed by applying a XeF_2 dry etch to the silicon substrate.

1.3 Si_3N_4 microresonator

Fig. 1b shows an SEM image of the Si_3N_4 (SiN) microresonator which is described in detail in Briles et al. [5]. The SiN resonator is fabricated by first depositing a thin layer (≈615 nm) of Si_3N_4 on a thermally-oxidized silicon wafer using low-pressure, chemical-vapor deposition. The 46 μm diameter ring resonator and coupling waveguides are then patterned using electron-beam lithography and formed using a dry etching process.

As is the case with the silica resonator, the SiN comb characteristics depend strongly on the resonator dispersion, which we control via the resonator geometry. For example, the carrier offset frequency can be controlled by varying the ring radius while the spectral location of the dispersive waves (as in Fig. 2) can be controlled by varying the thickness of the Si_3N_4 layer, the width of the ring and the final resonator cladding (air or oxide layer).

Shift	**Frac. Coef.**	**Shift (kHz)**	**Frac. Freq. Unc.**
AC Stark (meas.)	-3.9×10^{-12}/mW	-6.1×10^{-11}	7.8×10^{-15}
Rb-Rb coll. (meas.) [3]	-5×10^{-13}/K	-8.3×10^{-12}	5.0×10^{-12}
Bckgnd. gas coll. [3]			
Helium	5.5×10^{-9}/Torr	1.0×10^{-11}	2.2×10^{-12}
Other (e.g. N_2)	-3.5×10^{-8}/Torr	-3.9×10^{-12}	1.7×10^{-11}
2nd-order Zeeman [4]	6.5×10^{-11}/G^2	5.2×10^{-15}	6.5×10^{-15}
2nd-order Doppler	-1.0×10^{-15}/K	-3.6×10^{-13}	1.0×10^{-18}
Blackbody rad. [5]	-1.3×10^{-15}/K	-4.3×10^{-13}	1.5×10^{-15}
Electronic	$\sim3.2\times10^{-12}$/mV		$\sim1\times10^{-11}$
Total frac. uncer.			$\mathbf{2\times10^{-11}}$

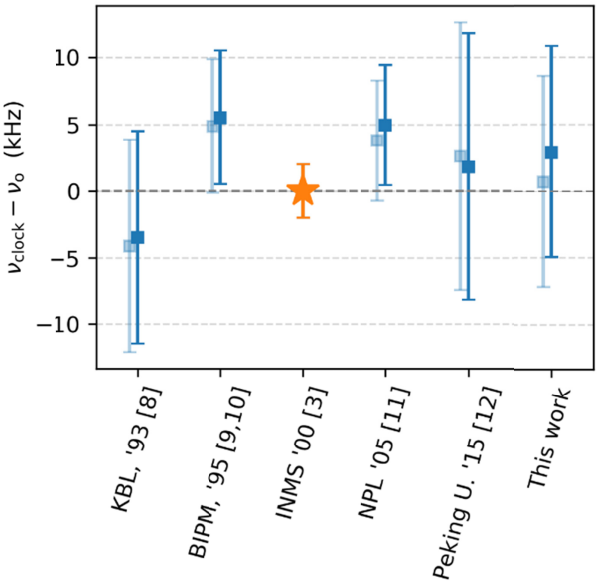

Fig. S1. Absolute frequency measurements of the $5S_{1/2}\rightarrow5D_{5/2}$, F=2 to F'=4 transition in ^{87}Rb relative to the BIPM adopted value for this transition (orange star) [3]. The light blue, offset squares show the absolute frequencies reported in the literature [3, 8–12]; darker blue squares show the corrected frequencies normalized to the rubidium vapor pressure from Ref. [3].

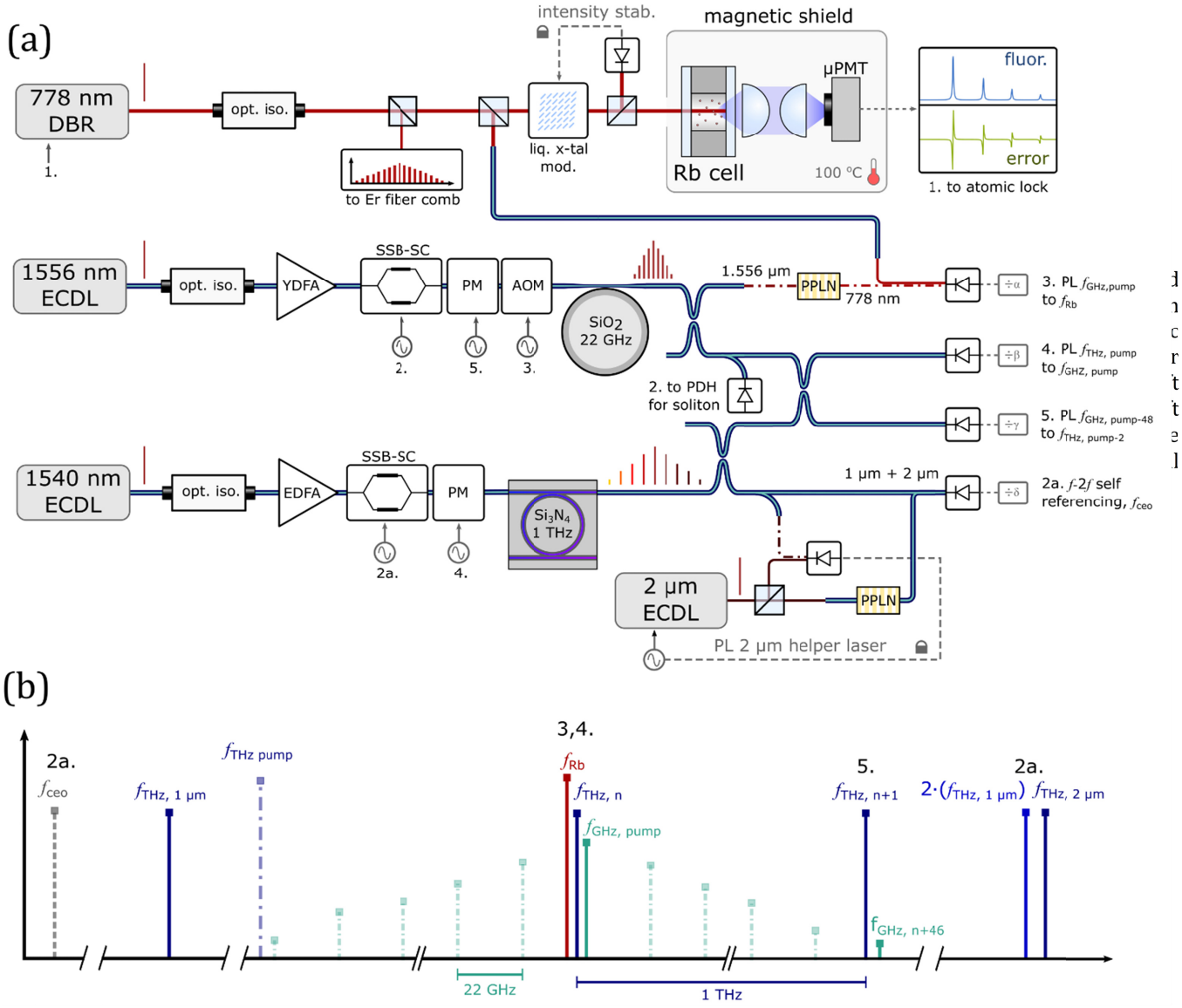

Fig. S2. (a) Detailed layout of the experiment. The phase locks for stabilizing the combs to the optical standard are indicated by numbers (1-5) in the order they are engaged during clock operation. Fiber paths, Dark/light blue lines; free-space paths, solid/dashed-dotted lines; electrical connections, grey dotted lines; PM, phase modulator; AOM, acousto-optical modulator; SSB-SC, single-sideband suppressed-carrier modulator; ECDL, external cavity diode laser; EDFA, erbium doped fiber amplifier; YDFA, ytterbium doped fiber amplifier; DBR, distributed Bragg-reflector; PMT, photomultiplier tube; PDH, Pound-Drever-Hall; PL, phase lock; PPLN, periodically-poled lithium niobite. (b) Diagram of the frequencies present in the clock laser/interlocked comb system. Here, solid (dashed) lines represent optical (microwave) frequencies used to generate beats for phase locking the combs. Dashed-dotted lines indicate comb lines not directly involved in comb stabilization. Numbers correspond to the locks described in the text and depicted in (a).

2. Clock output stabilization: Fig. S2 (a) gives a detailed layout of the optical clock subsystems. The electronic locks used to stabilize the clock laser and the two degrees of freedom of each microresonator comb are indicated in the figure by number in the order the locks are engaged during clock operation. Fig. S2 (b) shows a diagram of the optical frequencies used to stabilize the interlocked microcombs. Numbers above the optical lines correspond to the electronic locks in shown in (a)

2.1 Stabilized 778 nm laser system

The output of the clock laser is sent through an optical isolator and coupled into a polarization maintaining single mode optical fiber for spatial mode filtering. Following the fiber, a liquid crystal modulator is used to stabilize the optical power used to probe the rubidium atoms. The linearly polarized probe light is then focused to a spot size of 224 μm on the back window of the cell and retroreflected by the high-reflectivity coating on the back window.

We typically operate the rubidium standard with ≈16 mW of optical probe power. Fluorescence at 420 nm from the two-photon transition is collected along the probe beam axis with a pair of aspheric condenser lenses and a 420 nm bandpass interference filter and detected using a commercially available, microfabricated PMT.

To achieve a sufficient atomic density, the cell is heated to 100°C using a resistive heater driven with an alternating current to avoid magnetic bias fields near the cell. We stabilize the cell temperature to within 10 mK by feeding back to the amplitude of the alternating current. In addition, the heated cell mount, the PMT and the detection optics are housed inside a two-layer magnetic shield to minimize first order Zeeman shifts from stray magnetic field in the laboratory environment.

We stabilize the clock laser to the two-photon fluorescence spectrum using frequency modulation spectroscopy (Fig. S2: #1). The frequency of the clock laser is modulated at 10 kHz by directly modulating the DBR laser current with a modulation depth corresponding to a frequency excursion of ≈1 MHz. We generate an error signal using a lock-in amplifier to demodulate the observed fluorescence signal and lock the laser frequency by feeding back directly to the laser current.

As mentioned in the main text, we believe the short-term stability of our clock is limited by intermodulation noise from the DBR clock laser. The stability limit of a frequency standard due to the intermodulation effect can be approximated by [13]:

$$\sigma_y \sim \left[S_y(2f_{mod})/4\tau\right]^{1/2} \qquad \text{(S1)}$$

where $S(2f_{mod})$ is the oscillator frequency noise at twice the modulation frequency, in this case f_{mod} = 10 kHz. Fig. 4c shows a frequency noise spectrum of the DBR laser measured by beating against the fiber frequency comb. The DBR laser frequency noise at $2f_{mod}$ is $2\text{x}10^6$ Hz^2/Hz, which corresponds to an intermodulation limited stability of $\sigma_y \sim 2\text{x}10^{-12}/\tau^{1/2}$ and is consistent with our measured short-term stability. The short-term stability can be improved by utilizing low-noise sources for the clock laser. In fact, we have measured fractional stabilities of $\approx 4.5\text{x}10^{-13}/\tau^{1/2}$ using a commercial, 778 nm external cavity diode laser.

Roughly ≈1-2 mW of the stabilized clock laser is sent though an optical fiber and used to stabilize the pump frequency of the two microcombs. Additionally, ≈1 mW of the clock light is directed into a second optical fiber and beat against an auxiliary 250 MHz repetition rate, erbium fiber frequency comb to directly monitor the clock laser optical frequency.

2.2 Dual comb stabilization procedure

Our technique for generating single soliton combs in microresonators is described in detail in Stone et al. [14]. Briefly, we create a soliton frequency comb in the resonator by sweeping the pump frequency through the cavity resonance (from blue to red) with a single side band-suppressed carrier (SSB-SC) electro-optic phase modulator. The cavity supports the formation of solitons for a limited range of pump-resonator detunings, known as the soliton existence range, which is proportional to the linewidth of the cavity [15, 16]. As light is coupled into the resonator, the cavity resonance frequency shifts due to the thermo-optic effect [17]. As long as the thermal frequency drift stays within the soliton existence range, open loop control of the cavity detuning is sufficient to maintain a soliton. This is the case for the SiN resonator.

The linewidth of the silica resonator is substantially narrower, and, as a result, we lock the cavity detuning to compensate for the thermally induced shift. To accomplish this, RF sidebands are applied to the pump frequency and used to generate a Pound-Drever-Hall (PDH) error signal that is measured on a photo-detector at the output of the comb. We stabilize the soliton comb by locking the pump frequency detuning from the cavity resonance by feeding back to the setpoint of the SSB-SC modulator (Fig. S2: #2). The lock point of the PDH servo corresponds to the high-frequency PDH sideband and results in a pump frequency that is red-detuned from the cavity resonance by the RF modulation frequency, which is required for soliton generation. The modulation frequency (and resulting cavity detuning) is chosen such that the pump frequency is nominally independent of changes in the cavity detuning. The center frequency of the soliton comb can then be controlled by thermally tuning the optical path length of the cavity with an external heater.

During clock operation we frequency double the silica comb pump light to 778 nm and beat it against the rubidium stabilized DBR laser light (Fig. S2: lock #3). The ≈1.5 GHz ($\alpha \cdot f_{10\,\text{MHz}}$) beat note between the two lasers is used to phase lock the comb pump light by feeding back to an acousto-optical modulator (AOM) and controlling the intracavity power which, in turn, thermally shifts the cavity resonance. Next, we phase lock (Fig. S2: #4) the SiN comb tooth $\nu_{\text{THz, pump-2}}$ to $\nu_{\text{GHz,pump}}$ by controlling the pump frequency with the SSB-SC ($\beta \cdot f_{10\,\text{MHz}}$). The SiN comb is self-referenced (Fig. S2: #2a) by locking an auxiliary 2-micron ECDL to the SiN comb mode at 1998 nm, frequency doubling this light, beating the doubled light with the SiN comb tooth at 999 nm and feeding back to the SiN comb pump laser power with a SSB modulator ($\delta \cdot f_{10\,\text{MHz}}$).

Finally, we phase lock (Fig. S2: #5) the silica comb tooth $\nu_{\text{GHz,pump-48}}$ to the $\nu_{\text{THz, pump-3}}$ tooth of the SiN comb ($\gamma \cdot f_{10\ \text{MHz}}$) by controlling the RF sideband modulation frequency, and thus, the silica comb pump detuning, which is strongly coupled to the comb repetition rate via the soliton self-frequency shift [17].

References

1. A. Douahi, L. Nieradko, J. C. Beugnot, J. Dziuban, H. Maillote, S. Guerandel, M. Moraja, C. Gorecki, V. Giordano, "Vapour microcell for chip scale atomic frequency standard.," Electron. Lett. **43**, 279 (2007).

2. N. D. Zameroski, G. D. Hager, C. J. Erickson, J. H. Burke, "Pressure broadening and frequency shift of the 5S 1/2 to 5D 5/2 and 5S 1/2 to 7S 1/2 two photon transitions in 85 Rb by the noble gases and N 2.," J. Phys. B At. Mol. Opt. Phys. **47**, 225205 (2014).

3. J. E. Bernard, A. A. Madej, K. J. Siemsen, L. Marmet, C. Latrasse, D. Touahri, M. Poulin, M. Allard, M. Tetu, "Absolute frequency measurement of a laser at 1556 nm locked to the 5S1/2-5D5/2 two-photon transition in 87-Rb.," Opt. Commun. **173**, 357–364 (2000).

4. K. Y. Yang, K. Beha, D. C. Cole, X. Yi, P. Del'Haye, H. Lee, J. Li, D. Y. Oh, S. A. Diddams, S. B. Papp, K. J. Vahala, "Broadband dispersion-engineered microresonator on a chip.," Nat. Photonics. **10**, 316–320 (2016).

5. T. C. Briles, J. R. Stone, T. E. Drake, D. T. Spencer, C. Frederick, Q. Li, D. A. Westly, B. R. Illic, K. Srinivasan, S. A. Diddams, S. B. Papp, "Interlocking Kerr-microresonator frequency combs for microwave to optical synthesis.," Opt. Lett. **43**, 2933–2936 (2018).

6. K. W. Martin, G. Phelps, N. D. Lemke, M. S. Bigelow, B. Stuhl, M. Wojcik, M. Holt, I. Coddington, M. W. Bishop, J. H. Burke, "Compact Optical Atomic Clock Based on a Two-Photon Transition in Rubidium.," Phys. Rev. Appl. **9**, 014019 (2018).

7. M. Poulin, C. Latrasse, D. Touahri, M. Têtu, "Frequency stability of an optical frequency standard at 1926 THz based on a two-photon transition of rubidium atoms.," Opt. Commun. **207**, 233–242 (2002).

8. F. Nez, F. Biraben, R. Felder, Y. Millerioux, "Optical frequency determination of the hyperfine components of the two-photon transitions in rubidium.," Opt. Commun. **102**, 432–438 (1993).

9. L. Hilico, R. Felder, D. Touahri, O. Acef, A. Clairon, F. Biraben, "Metrological features of the rubidium two-photon standards of the BNM-LPTF and Kastler Brossel Laboratories.," Eur. Phys. J. Appl. Phys. **4**, 219–225 (1998).

10. R. Felder, D. Touahri, O. Acef, L. Hilico, J.-J. Zondy, A. Clairon, B. de Beauvoir, F. Biraben, L. Julien, F. Nez, Y. P. Millerioux, "Performance of a GaAlAs laser diode stabilized on a hyperfine component of two-photon transitions in rubidium at 778 nm.," Laser Freq. Stab. Noise Reduct. **2378**, 52 (1995).

11. C. S. Edwards, G. P. Barwood, H. S. Margolis, P. Gill, W. R. C. Rowley, "Development and absolute frequency measurement of a pair of 778 nm two-photon rubidium standards.," Metrologia. **42**, 464–467 (2005).

12. S. Y. Zhang, J. T. Wu, Y. L. Zhang, J. X. Leng, W. P. Yang, Z. G. Zhang, J. Y. Zhao, "Direct frequency comb optical frequency standard based on two-photon transitions of thermal atoms.," Sci. Rep. **5**, 15114 (2015).

13. C. Audoin, V. Candelier, N. Dimarcq, "A limit to the frequency stability of passive frequency standards due to an intermodulation effect.," IEEE Trans. Instrum. Meas. **40**, 121–125 (1991).

14. J. R. Stone, T. C. Briles, T. E. Drake, D. T. Spencer, D. R. Carlson, S. A. Diddams, S. B. Papp, "Thermal and Nonlinear Dissipative-Soliton Dynamics in Kerr-Microresonator Frequency Combs.," Phys. Rev. Lett. **121**, 63902 (2018).

15. X. Yi, Q.-F. Yang, K. Y. Yang, M.-G. Suh, K. Vahala, "Soliton frequency comb at microwave rates in a high-Q silica microresonator.," Optica. **2**, 1078–1085 (2015).

16. E. Lucas, H. Guo, J. D. Jost, M. Karpov, T. J. Kippenberg, "Detuning-dependent properties and dispersion-induced instabilities of temporal dissipative Kerr solitons in optical microresonators.," Phys. Rev. A. **95**, 043822 (2017).

17. T. Carmon, L. Yang, K. J. Vahala, "Dynamical thermal behavior and thermal self-stability of microcavities.," Opt. Express. **12**, 4742 (2004).